Cell

The Molecular Basis of CRL4$^{DDB2/CSA}$ Ubiquitin Ligase Architecture, Targeting, and Activation

Eric S. Fischer,[1,7,8] Andrea Scrima,[1,8,9] Kerstin Böhm,[1] Syota Matsumoto,[2] Gondichatnahalli M. Lingaraju,[1] Mahamadou Faty,[1] Takeshi Yasuda,[3] Simone Cavadini,[1] Mitsuo Wakasugi,[4] Fumio Hanaoka,[5] Shigenori Iwai,[6] Heinz Gut,[1] Kaoru Sugasawa,[2] and Nicolas H. Thomä[1,*]

[1]Friedrich Miescher Institute for Biomedical Research, Maulbeerstrasse 66, CH-4058 Basel, Switzerland
[2]Biosignal Research Center, and Graduate School of Science, Kobe University, 1-1 Rokkodai, Nada-ku, Kobe 657-8501, Japan
[3]National Institute of Radiological Sciences, 4-9-1 Anagawa, Inage-ku, Chiba 263-8555, Japan
[4]Laboratory of Human Molecular Genetics, Graduate School of Natural Science and Technology, Kanazawa University, Kakuma-machi, Kanazawa 920-1192, Japan
[5]Faculty of Science, Gakushuin University, 1-5-1 Mejiro, Toshima-ku, Tokyo 171-8588, Japan
[6]Graduate School of Engineering Science, Osaka University, 1-3 Machikaneyama, Toyonaka, Osaka 560-8531, Japan
[7]Universität Basel, Petersplatz 10, CH-4003 Basel, Switzerland
[8]These authors have contributed equally to this work
[9]Present address: Department of Molecular Structural Biology, Helmholtz-Centre for Infection Research, Inhoffenstrasse 7, D-38124 Braunschweig, Germany
*Correspondence: nicolas.thoma@fmi.ch
DOI 10.1016/j.cell.2011.10.035

SUMMARY

The DDB1-CUL4-RBX1 (CRL4) ubiquitin ligase family regulates a diverse set of cellular pathways through dedicated substrate receptors (DCAFs). The DCAF DDB2 detects UV-induced pyrimidine dimers in the genome and facilitates nucleotide excision repair. We provide the molecular basis for DDB2 receptor-mediated cyclobutane pyrimidine dimer recognition in chromatin. The structures of the fully assembled DDB1-DDB2-CUL4A/B-RBX1 (CRL4^{DDB2}) ligases reveal that the mobility of the ligase arm creates a defined ubiquitination zone around the damage, which precludes direct ligase activation by DNA lesions. Instead, the COP9 signalosome (CSN) mediates the CRL4^{DDB2} inhibition in a CSN5 independent, nonenzymatic, fashion. In turn, CSN inhibition is relieved upon DNA damage binding to the DDB2 module within CSN-CRL4^{DDB2}. The Cockayne syndrome A DCAF complex crystal structure shows that CRL4$^{DCAF(WD40)}$ ligases share common architectural features. Our data support a general mechanism of ligase activation, which is induced by CSN displacement from CRL4^{DCAF} on substrate binding to the DCAF.

INTRODUCTION

The evolutionarily conserved CUL4 E3 ligase family, in concert with its DDB1 adaptor, regulates a diverse set of cellular processes including development, transcription, replication and DNA repair (Jackson and Xiong, 2009). Specificity is conferred by a set of more than 50 WD40 containing substrate receptors, also referred to as DCAFs (*D*DB1 *C*UL4 *A*ssociated *F*actors) (Angers et al., 2006; Bennett et al., 2010; He et al., 2006; Higa et al., 2006; Jin et al., 2006). A large fraction of these targeting modules is directed toward chromatin-associated proteins. One of the best characterized substrate receptors is the damaged DNA binding protein 2 (DDB2), which binds to UV-induced DNA pyrimidine dimers. The DDB2 receptor is part of the DDB1-DDB2-CUL4-RBX1 E3 ligase complex (CRL4^{DDB2}) (Scrima et al., 2011). This bi-functional damage detection and ubiquitin ligase complex serves in the repair of UV induced DNA lesions in chromatin.

Exposure of the genomic DNA to ultraviolet light (UV) results in the formation of covalent crosslinks between neighboring pyrimidine nucleotides. These pyrimidine dimers, if left unrepaired, stall transcription by RNA polymerase II (RNAPII). Unrepaired lesions require error-prone translesion polymerases in S phase (Friedberg, 2001), which potentially introduce oncogenic mutations. Cyclobutane pyrimidine dimers (CPD) and (6-4) pyrimidine-pyrimidone photoproducts (6-4PP) are the two major photo-lesions, accounting for approximately 75% and 25% of genomic UV lesions, respectively (Mitchell et al., 1989). Compared to 6-4PP, CPDs cause relatively minor thermodynamic duplex destabilization (Jing et al., 1998), and are found frequently obscured by organization into nucleosomes (Gale and Smerdon, 1988). These biophysical and cellular properties render CPDs the most difficult photo-lesion to detect. CPDs are thereby highly mutagenic and major facilitators of skin carcinogenesis (Hoeijmakers, 2009).

The mammalian global genome repair branch of nucleotide excision repair (NER) surveys the genome for lesions and actively

repairs pyrimidine dimers (Aboussekhra et al., 1995). NER thereby functions as a central pathway in safeguarding metazoan cells against sun-induced skin carcinogenesis. XPC-RAD23-Centrin2 acts as a lesion surveillance complex, recruiting the core NER machinery to damaged sites (Volker et al., 2001). Assembly of the NER complex results in rapid damage excision and repair synthesis, with repair generally proceeding in a fast and error-free fashion. While XPC is required for global genome NER, it has little or no affinity for CPD lesions, and does not recognize 6-4PP in the context of chromatin (Batty et al., 2000; Sugasawa et al., 2001; Yasuda et al., 2005). Recently, XPC recruitment to chromatin was shown to be facilitated by the DDB1-DDB2 (UV-DDB) complex (Nishi et al., 2009). In the absence of DDB2, XPC remains localized to 6-4PP and to a lesser extent to CPDs, albeit with substantially delayed kinetics (Sugasawa, 2010). The precise mechanism of XPC recruitment to sites of UV damage, in the absence of DDB2 is unclear. DDB2 binds to CPD and 6-4PP pyrimidine dimers with the highest reported affinity and specificity of all metazoan damage recognition factors (Payne and Chu, 1994; Wittschieben et al., 2005). Mutations in DDB2 give rise to XP complementation group E (Tang and Chu, 2002). In DDB2-deficient XPE cells, CPD repair is largely abolished, while 6-4PP repair is affected to a lesser extent (Hwang et al., 1998; Moser et al., 2005; Tang et al., 2000). The structural basis of 6-4PP recognition by DDB1-DDB2 is known (Scrima et al., 2008) but it is currently unclear how DDB2 recognizes CPD lesions, which are chemically distinct from the 6-4PP and frequently encapsulated in nucleosomes (Gale and Smerdon, 1988).

DDB1-DDB2 appears constitutively bound to CUL4 which targets XPC and DDB2 for ubiquitination (Sugasawa et al., 2005). In addition, histones H2A, H3 and H4 surrounding the lesion are ubiquitinated in a UV-dependent fashion (Guerrero-Santoro et al., 2008; Kapetanaki et al., 2006; Wang et al., 2006). DDB2 autoubiquitination leads to the loss of DNA damage binding and rapid DDB2 degradation (Sugasawa et al., 2005). XPC ubiquitination, in contrast, retains the complex at the site of UV damage without immediate proteasomal degradation. The differential response of XPC and DDB2 upon ubiquitination has been linked to a ubiquitin-dependent damage handover from $CRL4^{DDB2}$ to XPC (Sugasawa et al., 2005). $CRL4^{DDB2}$ is found in complex with the COP9 signalosome (CSN) (Hannss and Dubiel, 2011). CSN is an 8-subunit isopeptidase complex, which via the proteolytic activity of its CSN5 subunit removes the ubiquitin-like NEDD8 from cullins. NEDD8 is considered as an activator and its removal renders the ligase complex inactive (Furukawa et al., 2000). Recruitment of $CRL4^{DDB2}$ to sites of DNA damage in chromatin appears to correlate with CSN release (Groisman et al., 2003; Takedachi et al., 2010). The molecular mechanism triggering $CRL4^{DDB2}$ activation in response to damage binding is currently unresolved.

While the DDB2 substrate receptor recruits $CRL4^{DDB2}$ to DNA damage, other CRL4 substrate receptors are recruited by protein epitopes. Prominent examples include DCAF1, CDT2 and the Cockayne syndrome A (CSA) protein (Lee and Zhou, 2007). All CRL4 substrate receptors are linked to CUL4 through the DDB1 adaptor. CSA is functionally unrelated to DDB2 and serves in the transcription coupled branch of NER. $CRL4^{CSA}$ is recruited to sites of CSB and stalled RNA polymerase II, where it facilitates DNA repair and the subsequent transcription restart (Tornaletti, 2009). Reported $CRL4^{CSA}$ ubiquitination targets include the Cockayne syndrome B protein (CSB), a SWI/SNF ATPase (Troelstra et al., 1992). $CRL4^{DDB2}$ and $CRL4^{CSA}$, as well as other cullin-RING type ligases are inhibited by CSN (Bennett et al., 2010). It is currently unclear how CSN inhibition is retained at the majority of cellular cullin ligase complexes, while CSN specifically dissociates from those ligases that undergo activation in response to a given stimulus (i.e.: CSN mediated dissociation and activation of $CRL4^{DDB2}$ and $CRL4^{CSA}$ in response to UV).

Here, we provide the molecular basis for $CRL4^{DDB2}$ recruitment to CPD lesions in chromatin, and characterize how the damage recognition process results in ubiquitin ligase activation, a process mediated by CSN. We present the structure of the DDB1-CSA complex, which in conjunction with biochemical data presented argues in favor of conserved architectural and regulatory principles among CRL4 ligases.

RESULTS

CPD Recognition by DDB2 Involves β-Hairpin Insertion and Lesion Flipping

The DDB2 damage detection module has previously been postulated to undergo conformational changes upon binding of a pyrimidine dimer resulting in $CRL4^{DDB2}$ activation in vivo (Takedachi et al., 2010). We therefore focused on the structure of the DDB1-DDB2 complex bound to CPD-containing duplexes, its physiological substrate. DDB1-DDB2 has the highest reported affinity for CPD lesions among metazoan damage recognition factors. Its absolute affinity, however, was not sufficient to allow successful crystallization in the presence of CPD duplexes. We then engineered DDB1-DDB2 crystal contacts disfavoring crystallization of the DNA-free (apo) state, biasing crystallization toward CPD cocomplexes. This was done by mutating DDB1 contacts that occur only in the apo-DDB1-DDB2 crystal lattice, as DDB1 is not involved in DNA binding (Figure S1 available online). This approach led to the structures of DDB1-DDB2 bound to four different cis-syn CPD-containing DNA duplexes, observed in different space groups and crystal packing arrangements (Figure 1; Figure S1). Due to the overall structural similarity among these DNA cocomplex structures, the discussion focuses on the 3.0 Å resolution structure of DDB1-DDB2 bound to a 13-mer duplex having a 5′ overhang on both strands (CPD#1).

Consistent with the DDB1-DDB2 6-4PP complex (Scrima et al., 2008), the CPD-containing duplex is exclusively held by the DDB2 WD40 propeller. The DNA traverses the central cavity of the WD40 propeller along the axis defined by DDB2 blades 7 and 4, pointing away from DDB1 (Figure 1). A DDB2 β-hairpin, comprising Phe371, Gln372 and His373 is inserted into the minor groove of the duplex at the site of the CPD. Insertion of this damage-recognition finger (Scrima et al., 2008) proceeds with duplex unwinding of ~12.6° (Figure S1D), widening of the minor groove to ~18 Å (Table S2) and extrusion of the CPD into an extra-helical, flipped out conformation. The observed kink angle of the cis-syn CPD DNA in the highest resolution CPD complex is ~45°.

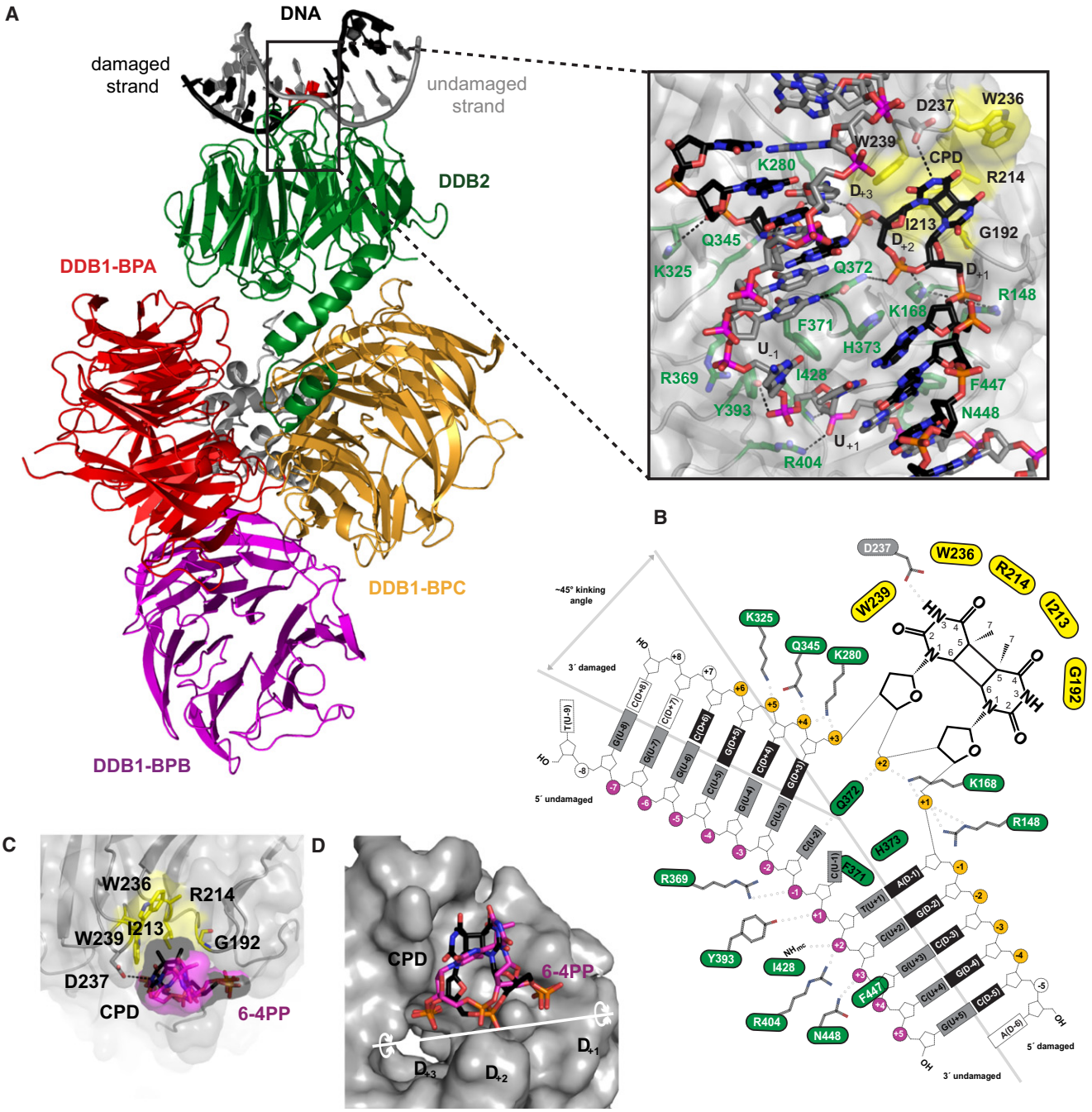

Figure 1. DDB1-DDB2 in Complex with CPD-Containing Duplexes

(A) Cartoon representation of DDB1-DDB2-CPD. DDB2, green; DDB1 (BPA), red; (BPB), magenta; (BPC), yellow; DDB1-CTD, gray and the DNA in black and gray for the damaged and undamaged strand respectively, with CPD shown in red. The DDB2 residues involved in DNA binding are shown as close-up.

(B) Schematic representation of DNA-protein interactions.

(C) Close-up view of the CPD/6-4PP fit to the hydrophobic binding pocket. (D) Close-up of the bound CPD lesion, demonstrating that the DDB2 binding pocket preferentially accommodates the CPD.

See also Figure S1 and Tables S2 and S3.

The DDB2 Binding Interface Is Specifically Tailored toward CPD Recognition

The 6-4PP structure previously revealed few contacts between DDB2 and the extruded 6-4PP (Scrima et al., 2008). The 6-4PP has the pyrimidine-pyrimidone rings angled at ~90° and can therefore not fully engage the DDB2 damage recognition pocket (Figures 1C and 1D). The boat-shaped cis-syn CPD, in contrast, provides a high degree of surface complementarity through

packing with its hydrophobic carbons (at C5 and C6 positions) against the hydrophobic core of the DDB2 pocket (Figure 1). This interaction is stabilized by DDB2 residues Trp239, Ile213, Gly192, and the Cα of Arg214. The four hydrophilic carbonyl groups of the CPD (at the C2/C4 positions), located on the opposing face, are solvent exposed and contact water molecules. The carboxylic group of Asp237 contacts the D_{+2} pyrimidine nitrogen at N3. The overall arrangement results in a larger contact area of 327 $Å^2$ for the CPD moiety versus 265 $Å^2$ for the 6-4PP.

Comparison with existing structures of protein-free CPD duplexes indicated that the DNA conformation seen in the DDB2-CPD complex (Figure 1) closely resembles previously observed protein-free cis-syn CPD duplexes (Figure S1). DDB2, through its pyrimidine dimer binding pocket and overall DNA shape complementarity, thereby specifically supports CPD recognition.

The DDB1-DDB2 Complex Does Not Change Its Conformation in Response to Damage Binding

The DDB2 6-4PP, THF (Scrima et al., 2008) and CPD structures illustrate that the DNA is intrinsically flexible and can adapt to DDB2 despite differences in the DNA sequence (see Figure S1). The plasticity of the DNA is contrasted with the rigidity of DDB2. In all DNA bound and DNA free structures available, DDB2 including its β-hairpin does not change its conformation. Thus, DDB2 serves as a rigid damage recognition unit. As a consequence DDB2 binding to its physiological CPD substrate does not trigger conformational changes that could serve as the signal in ligase activation (see below).

DDB2 Mediated Detection of CPD Lesions in Chromatin

The DDB2 DNA binding interface has previously been proposed to allow readout of lesions embedded in nucleosomes (Scrima et al., 2008). This is of notable biological importance, as the majority of CPDs appear encapsulated in nucleosomes (Gale and Smerdon, 1988). The DNA curvature observed when bound to DDB2 matches the nucleosomal curvature (Scrima et al., 2008) which was proposed to facilitate pyrimidine dimer readout through the minor groove. In order to test whether the DDB2 interface is compatible with nucleosomal damage detection, damage-containing nucleosomes were initially prepared by UV irradiation of DNA prior to the assembly of core particles (Extended Experimental Procedures). Electrophoretic mobility shift assays (EMSA) (Extended Experimental Procedures) demonstrated that DDB1-DDB2 is able to specifically recognize irradiated, linker free, mononucleosomes (Figure 2A). We subsequently prepared nucleosomes containing a chemically synthesized 6-4PP or CPD lesion (Figures 2B and 2C). Driven by nucleosome positioning sequence consisting of alternating A/T- and G/C-rich regions, these lesions were located at the sites where the minor groove is oriented away from the surface of the histone octamer (Yasuda et al., 2005). DDB1-DDB2 recognizes a single 6-4PP embedded in the nucleosome (Figure 2B, lanes 10–12) and comparable binding can be observed in the presence of the equal amount of 6-4PP-containing naked DNA (Figure 2B, lanes 13–16). Binding was also detected for the CPD-containing nucleosomes (Figure 2C). CPD nucleosome binding was weaker than that of the 6-4PP (Figures 2D and 2E), in line with its intrinsically lower helix destabilization (Jing et al., 1998). Binding of CPD-containing nucleosomes was comparable, however, with DDB2 affinities observed for naked CPD-containing DNA. The DDB2 DNA binding interface in addition to being optimized for CPD recognition, also confers compatibility for detecting CPDs and 6-4PPs in nucleosomes.

Measurements of cellular diffusion rates identified the $CRL4^{DDB2}$ complex as the functional macromolecular entity in DDB2 mediated DNA damage recognition (Luijsterburg et al., 2007). We therefore examined binding of the fully assembled $CRL4^{DDB2}$ complex to irradiated nucleosomes (Figure 2F). Analogous to our findings with DDB1-DDB2, we observed that the $CRL4^{DDB2}$ complex is able to specifically recognize lesions in nucleosomes, suggesting that the presence of CUL4 is compatible with damage recognition in chromatin. In an effort to understand the interplay between damage binding and ligase activation, we subsequently focused on the structure of the $CRL4^{DDB2}$ complex bound to damaged DNA duplexes.

Structures of DDB1-DDB2-CUL4A/B-RBX1 Bound to Damage-Containing Duplexes

We first determined the structure of DDB1-DDB2-CUL4A-RBX1 ($CRL4A^{DDB2}$) bound to a 12 bp DNA duplex containing a tetrahydrofuran (THF) lesion, a well characterized DDB2 substrate (Wittschieben et al., 2005). The structure of this 290 kDa nucleoprotein complex was refined by rigid body refinement to 5.9 Å resolution with an R_{work} of 26.9% (R_{free} of 27%) as outlined in Extended Experimental Procedures. Fragments from previously available high resolution structures of CUL4A (Angers et al., 2006), DDB1, DDB2, and DNA (Scrima et al., 2008) were positioned using iterative cycles of molecular replacement searches (Extended Experimental Procedures). The location of these individual rigid bodies was validated with anomalous dispersion methods using a selenomethionine (SeMet) labeled $CRL4A^{DDB2}$ complex. Phases derived from molecular replacement were used for calculation of anomalous difference Fourier electron density maps, which allowed identification of peaks for 50% of the 55 expected Se at 3.0 σ (90% at 2.0 σ). All peaks were located within 5 Å of their predicted position (Figure S2D). Calculation of composite omit maps with CNS (Brunger et al., 1998) further corroborated the correct placement of the different domains of the large complex (Figure S2C). Well defined 2 mF_{obs}-DF_{calc} density was observed for CUL4A, DDB1 (BPB, BPC&BPA), DDB2 (helix-loop-helix motif and WD40 propeller) and the 24 nucleotides of the DNA duplex. While density was present for the segment of RBX1 residues 19–39 that integrates into the CUL4A C-terminal β sandwich (Angers et al., 2006), no density was observed for the remainder.

Figure 3 shows the structure of $CRL4A^{DDB2}$ complex bound to a damage-containing duplex. $CRL4A^{DDB2}$ assumes an overall U-shaped assembly, with two extended arms of nearly equal length. The thicker arm is contributed by DDB1-DDB2 (extreme dimensions 75 Å x 45 Å), while the thinner arm comprises CUL4A (75 Å x 23 Å). The connection between them is made by the N terminus of CUL4A (aa 39–96) in conjunction with the DDB1-BPB domain (Angers et al., 2006). The DDB1-DDB2 and CUL4A extended arms are angled at about 50°. The overall complex assumes an approximately square arrangement

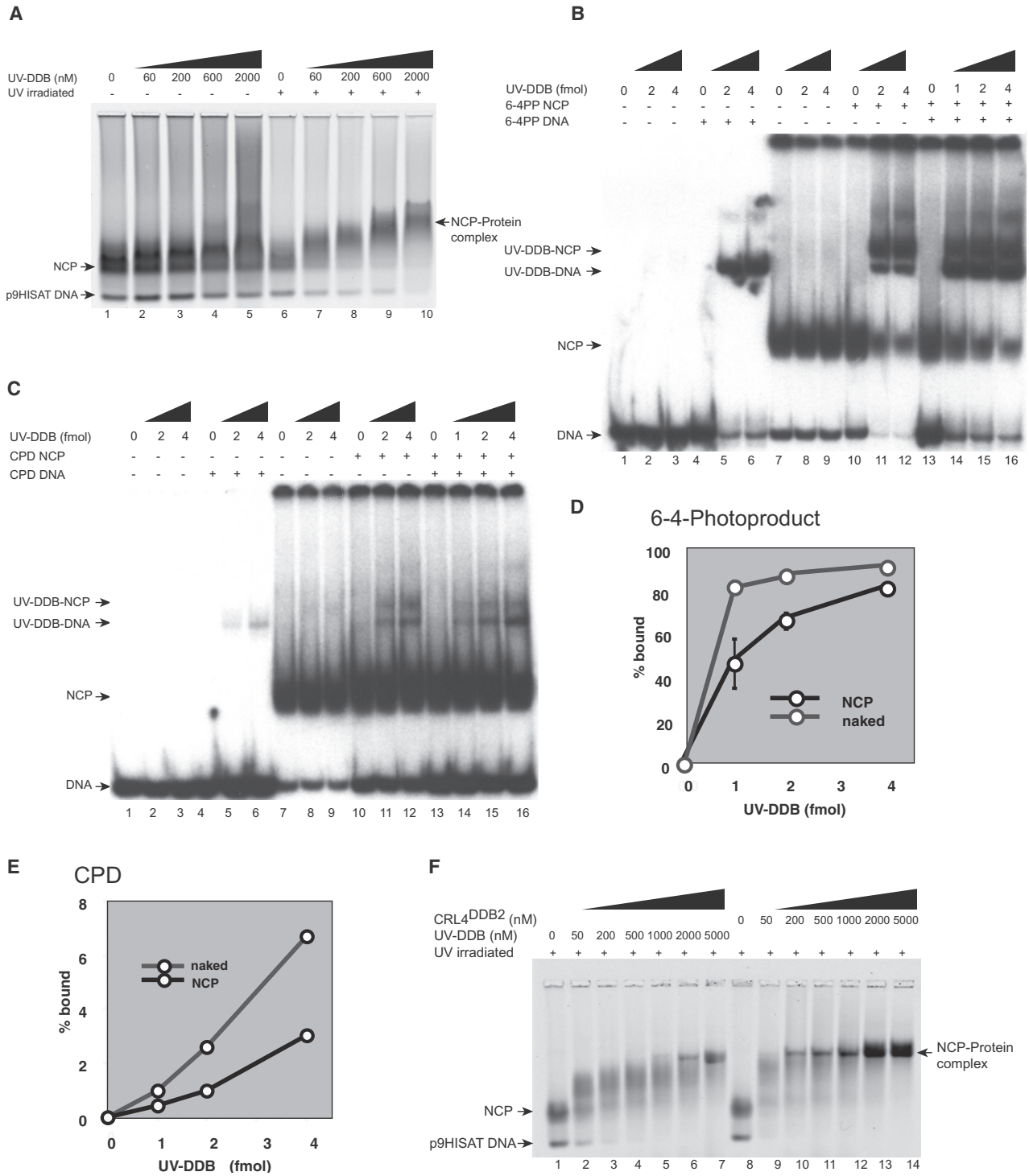

Figure 2. DDB2 Is Able to Recognize 6-4PP and CPDs Embedded in Nucleosomes

(A) EMSA of the DDB1-DDB2 complex binding to UV-damaged nucleosome core particles (NCP), indicated amounts of DDB1-DDB2 were incubated with UV-damaged or undamaged mononucleosomes.

(B) EMSA analysis of DDB1-DDB2 binding to nucleosomes containing a specific 6-4PP lesion, indicated amounts of DDB1-DDB2 were incubated with 0.2 fmol of naked DNA (lanes 1-6), mononucleosomes (lanes 7–12) or both (lanes 13–16). The nondamaged DNA control is shown as indicated.

(C) As in (B) using CPD containing nucleosomes.

(D) and (E) Quantitative analysis of DDB1-DDB2 binding to free lesion containing DNA or to a lesion embedded in the nucleosomes 6-4PP (B) or CPD (C). (F) EMSA analysis of DDB1-DDB2 and CRL4A^{DDB2} complex binding to UV-damaged mononucleosomes.

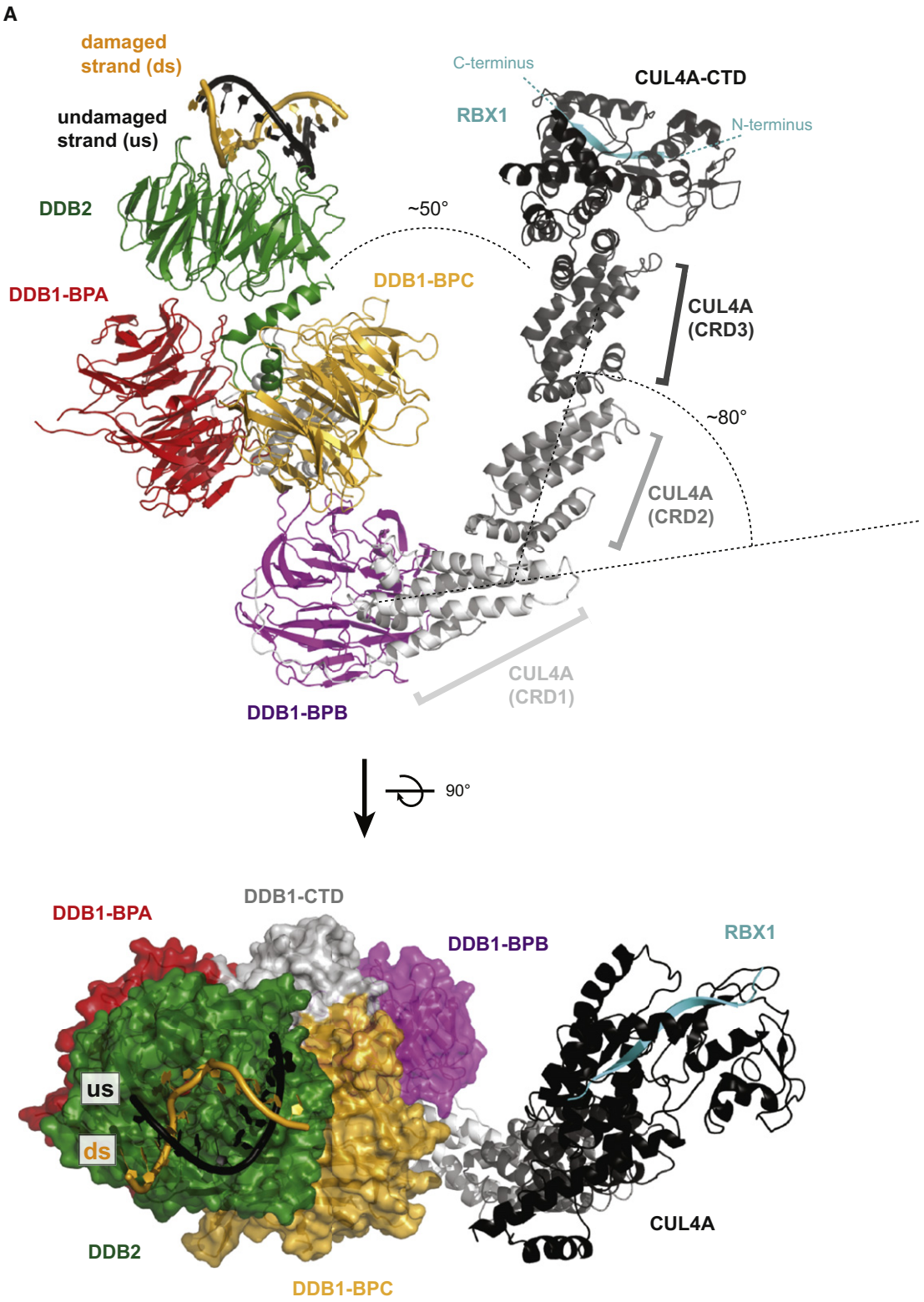

Figure 3. The Structure of the CRL4A^{DDB2} Complex Bound to THF-Containing Duplex

Cartoon representation of the CRL4A^{DDB2} complex structure: DDB2, green; DDB1 (BPA), red; (BPB), magenta; (BPC), orange, DDB1-CTD, gray; CUL4A, cullin repeat domains (CRD1-3) and C-terminal domain (CTD) depicted in gray to black; RBX1 in cyan. The DNA is shown in black and orange for the undamaged and damaged strand respectively. DDB1 and DDB2 are shown as surface in the bottom panel. See also Figure S2.

(160 Å x 140 Å). The largely helical CUL4A fold is attached exclusively to the BPB WD40 propeller of DDB1 (Figure 3). The observed distances between the CUL4A arm and the remainder of the DDB1 (BPC+BPA) propellers are generally more than 15-20 Å. The distance between CUL4A and the DNA duplex is around 50 Å. This arrangement excludes specific interactions between CUL4A and the DNA, or CUL4A and the BPA and BPC propellers of DDB1 (Figure 3).

The CUL4A and CUL4B Ligases Are Structurally Indistinguishable

Since human cells possess two CUL4 isoforms, CUL4A and CUL4B (Jackson and Xiong, 2009) with DDB1-DDB2 reported to exist in complex with both of them (Groisman et al., 2003; Wang et al., 2006), we determined the crystal structure of CUL4B-RBX1 bound to DDB1-DDB2 in the presence of a second 12 bp THF containing duplex DNA (7.4 Å resolution). While the cullin fold of CUL4B (aa 192–913) has high sequence identity to CUL4A (84% over 722 residues), the CUL4B N terminus is unique to CUL4B. The CUL4B aa 1–191 N terminus was predicted to be mostly unstructured and was removed prior to coexpression of the $CRL4^{DDB2}$ complex.

In the absence of known CUL4B structures, we first determined the structure of CUL4B (in complex with CAND1) at 3.8 Å resolution (Extended Experimental Procedures). Analysis of CUL4A and CUL4B folds revealed superimposable structures (rmsd of 1.54 Å over 677 residues) rendering the two homologs structurally indistinguishable (see Figure 4C and Figure S3 for the mapping of CUL4B mutations resulting in X-linked mental retardation).

The CUL4 E3 Ligase Freely Rotates Around a Rotation Axis Defined by DDB1 and the Damage

The structure of the DDB1-DDB2-CUL4B-RBX1 ($CRL4B^{DDB2}$) complex was solved following a similar strategy, as outlined for $CRL4A^{DDB2}$ (Extended Experimental Procedures). The overall architecture of the two $CRL4B^{DDB2}$ complexes, observed in the asymmetric unit was comparable with $CRL4A^{DDB2}$ (Figure 4). Clear density for RBX1, again was only visible for aa 19–39 in both molecules of $CRL4B^{DDB2}$. Comparison of the $CRL4A^{DDB2}$ with the two $CRL4B^{DDB2}$ molecules revealed the DDB1-BPB domain in three different rotational states. As the BPB domain is the anchor point of the CUL4 ligase, its mobility directly translates into the mobility of the entire ligase arm. Within the three molecules observed in our study (Figures 4A and 4B), CUL4 rotates around 60° along an axis defined by the damage and DDB1 (BPB propeller) (Figure 4). Minimal distances observed between CUL4B and DNA, and between CUL4B and DDB1 (BPC), for the two CUL4B molecules were between 25–35 Å and 5–27 Å, respectively. The cullin fold with its kink of ~80° between cullin repeats 1 and 2 is shaped to allow rotation over BPC blades 2 and 3 toward the DDB1 C terminus without steric clashes with DDB1 (Figure 4).

The DDB1 BPB Domain Mobility Structurally Insulates the CUL4 Ligase from the DDB2 Module

Examination of the 11 available medium/high resolution DDB1 molecules obtained in crystallographic studies (Angers et al., 2006; Li et al., 2006; Li et al., 2010; Scrima et al., 2008) suggest a total BPB domain rotation range of at least 150° (Figure 4D). Analysis of the expected energetics of rotation, as calculated by differences in solvation energy for the individual DDB1 (BPB) versus DDB1 (BPC-BPA) interfaces (Krissinel and Henrick, 2007) predicts that the observed rotations are iso-energetic (Figure 4E). As a consequence, $CRL4^{DDB2}$ is expected to rotate up to 150° establishing a ubiquitination zone restricted to 60–80 Å. Upon modification with the small ubiquitin like modifier NEDD8 and resultant release of RBX1, the ubiquitination zone increases to 30-110 Å (Duda et al., 2008) (Figure 4D).

The overall modular architecture of $CRL4^{DDB2}$ implies that CUL4 cannot be directly activated through conformational changes induced by DDB2 damage binding. The mobility of the ligase arm further insulates CUL4 from DDB2. Activation of the ligase in response to DNA damage therefore requires additional factors. We next focused on known regulators and their role in $CRL4^{DDB2}$ regulation.

The DDB2-N Terminus Is Autoubiquitinated and Regulates DDB2 Levels after UV Irradiation

The $CRL4^{DDB2}$ complex, in vivo, undergoes DDB2 autoubiquitination and degradation following UV irradiation. In contrast, the recombinant $CRL4^{DDB2}$ complex undergoes DDB2 autoubiquitination irrespective of the presence and absence of DNA damage. The DDB2 subunit has previously been shown to undergo polyubiquitination at multiple sites (Sugasawa et al., 2005). Using mass spectrometry, in conjunction with a ubiquitin variant lacking lysine residues required for polyubiquitination, we identified the human DDB2 Lys residues 5, 11, 35, 40 and 151 as the main targets for $CRL4^{DDB2}$ autoubiquitination in vitro (Figures S4A–S4D). The majority of these sites (Lys5, 11, 35 and 40) are located within the unstructured DDB2 N terminus. When determining the human DDB1-DDB2 complex structure DDB2 aa 1–59 were absent from the electron density maps, and were removed for subsequent structural studies. In vitro, deletion of the DDB2 N terminus, aa 1–40 ($DDB2_{\Delta N}$), ablated the majority of ubiquitin acceptor sites (Figure 5A). On the basis of random-polymer-theory (Creighton, 1992) the very N terminus of DDB2 is estimated to have a root-mean-square distance of about 90 Å from the beginning of the DDB2 structure (aa 1-66). The DDB2 N terminus is thereby located on the edge of the active ubiquitination zone of the ligase.

Next, we assessed the effect of these lysine residues in cells, in response to UV damage. A normal human fibroblast cell line, WI38 VA13, was used to stably express HA-tagged wild-type DDB2 or a construct in which 7 N-terminal lysines (at positions 4, 5, 11, 22, 35, 36, and 40) were mutated to arginines ($DDB2_{7KR}$). $DDB2_{7KR}$ remained associated with DDB1 and CUL4 in a manner identical to that seen for wild-type DDB2 (Figure 5B). After blocking translation by cycloheximide treatment and UV irradiation, $DDB2_{7KR}$ showed remarkable stability compared to the wild-type DDB2; cellular wild-type DDB2 levels mostly disappeared 1 hr after UV, whereas $DDB2_{7KR}$ levels remained unchanged for 5 hr (Figure 5C). Differences in total levels of wild-type DDB2 and $DDB2_{7KR}$ are visible as early as 30min post UV, at a time when CSN has previously been shown to dissociate from the complex (Groisman et al., 2003). Wild-type and $DDB2_{7KR}$

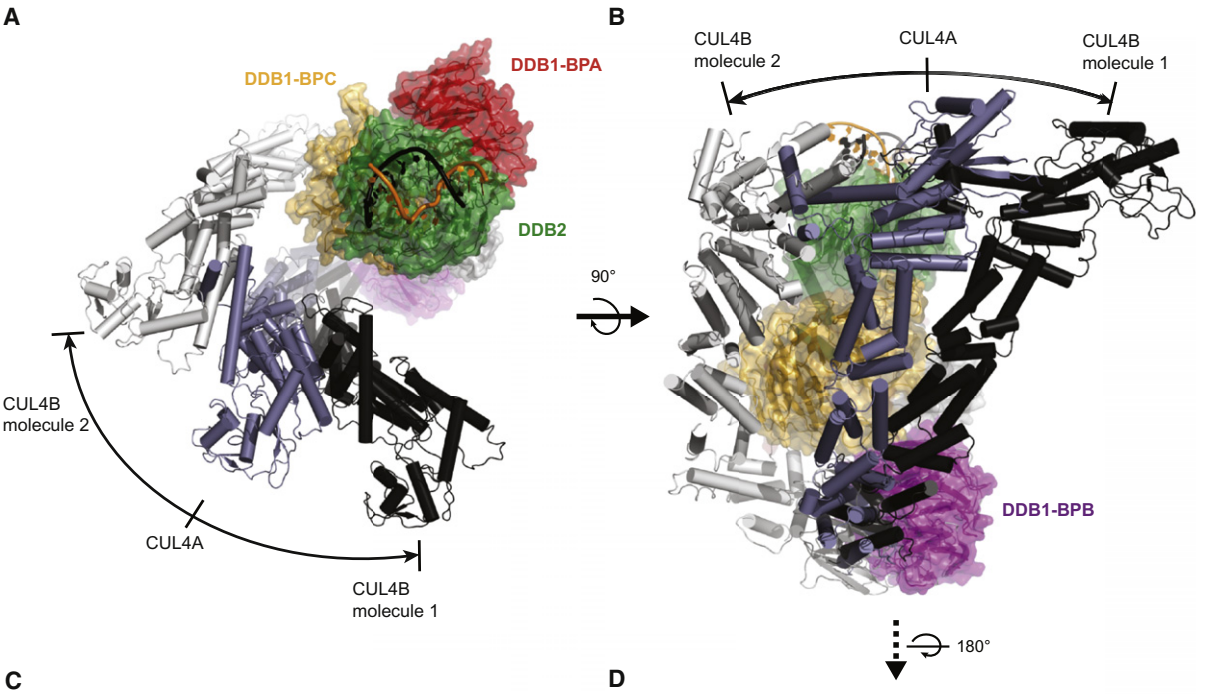

E

PDB	angle	ΔG (kcal/mol)
2HYE	0.0°	-1.3
3EI4 (mol1, 2, 3)	50.0°	-3.2
2B5L	53.9°	-2.3
3EI3	103.4°	0.0
3EOC	105.2°	-3.1
3EI1	113.3°	3.7
3EI2	117.3°	3.7
4A09	125.5°	1.5
2B5M	129.0°	4.7
3I7H	147.5°	0.9
4A0A	150.9°	3.2

Figure 4. The Structures of CRL4B^{DDB2} Bound to DNA Damage: Rotational Mobility of the Ligase

(A and B) Overlay of the three experimental CUL4 orientations indicating the rotational mobility of CUL4 (in gray) respective to DDB2 (depicted as surface in green) and the bound DNA substrate (depicted in orange and black).

(C) Overlay of medium to high resolution CUL4A and CUL4B structures and schematic representation of domain boundaries.

(D) Model of CRL4^{DDB2} with the CUL4 arm depicted in the most distal DDB1-BPB orientations and the resultant ubiquitination hot zone indicated in light orange and gray.

(E) Table of available medium to high resolution DDB1 structures with the corresponding orientation of CUL4 and predicted ePISA solvation energies of DDB1 (BPB) to DDB1 (BPA/BPC) interactions.

See also Figure S3.

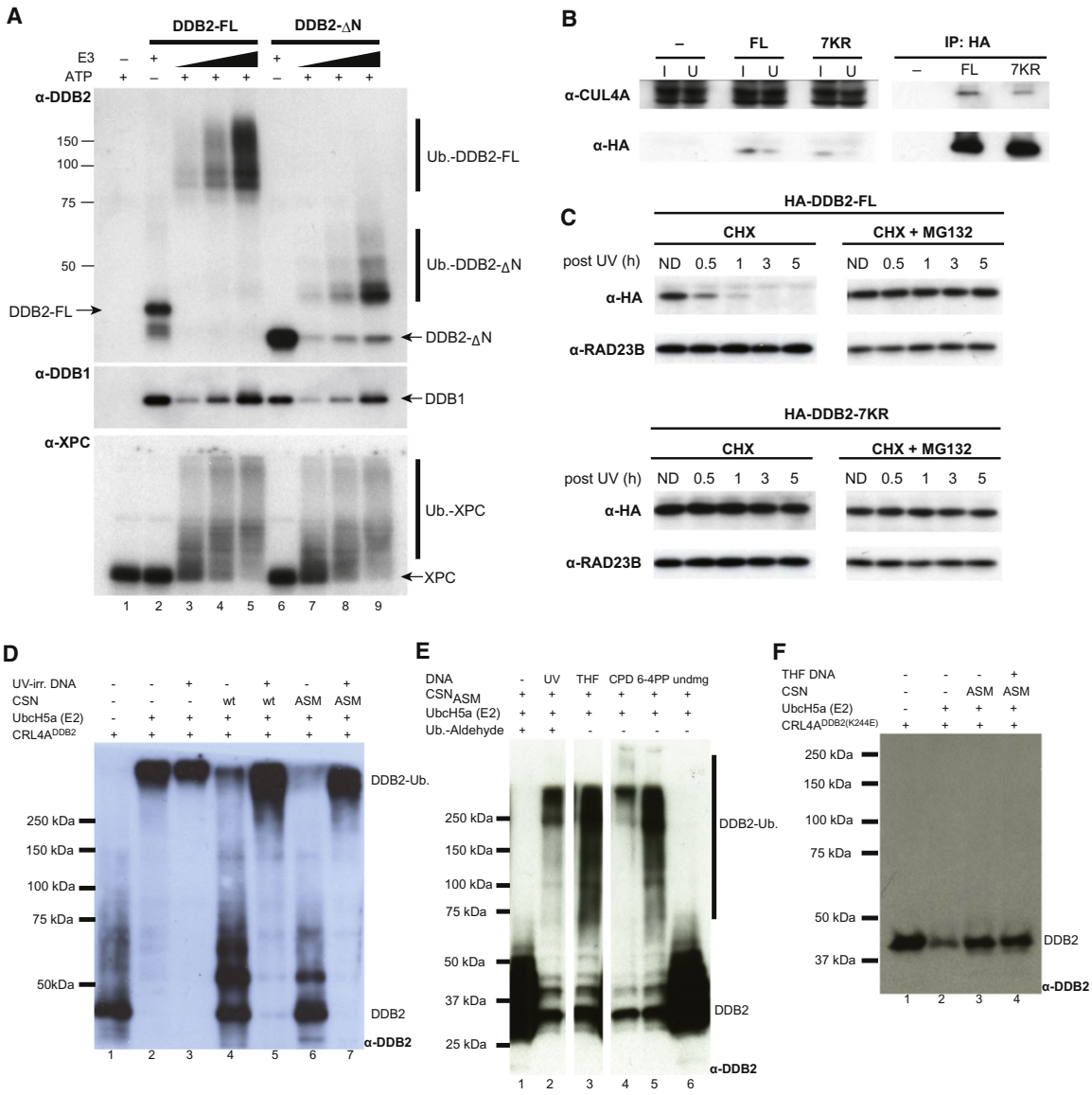

Figure 5. CSN-Dependent Regulation of CRL4^{DDB2}-Mediated Ubiquitination of the DDB2 N Terminus Regulates Degradation following UV Exposure

(A) In vitro ubiquitination assays using K-less ubiquitin and the CRL4A^{DDB2} complex containing either full-length DDB2 (DDB2-FL) or DDB2-ΔN. The reaction mixture was subjected to immunoblot analysis with indicated antibodies.

(B) HA-tagged DDB2-FL or DDB2-7KR was stably overexpressed in a normal human fibroblast cell line. Extracts from these cells as well as the parental cell line (indicated by -) were subjected to immunoprecipitation with anti-HA antibody and immunoblot analysis with indicated antibodies. One percent each of the input extracts (I) and unbound fractions (U) were analyzed in parallel.

(C) The cell line stably expressing HA-DDB2-FL or HA-DDB2-7KR was exposed to UV irradiation 2 hr after treatment with 1 mM cycloheximide (CHX) in the presence or absence of 5 μM MG132. Cells were further incubated for various times in the presence of CHX (±MG132) and whole cell extracts were subjected to immunoblotting using indicated antibodies.

(D) In vitro ubiquitination assays were performed with wild-type CRL4A^{DDB2} complex and analyzed by DDB2 immunoblot. Wild-type CSN complex (lane 4) or a complex containing a CSN5 active site mutant (lane 5) significantly inhibited the autoubiquitination of DDB2. This inhibition was relieved by the addition of UV-irradiated DNA to the reaction (lanes 5 and 7).

(E) Small oligonucleotides containing an THF abasic site mimic (lane 3), CPD lesion (lane 4) or 6-4PP lesion (lane 5) were sufficient to relieve the inhibition, whereas an undamaged oligonucleotide of similar length did not affect the inhibition (lane 6). Ubiquitin-aldehyde had no effect on the reaction (lane 1 and 2).

(F) In vitro ubiquitination assays were performed with CRL4A^{DDB2} complex harboring the K244E DDB2 patient mutation. In contrast to wt DDB2, the inhibition by CSN$_{ASM}$ was not relieved upon damaged DNA addition (lane 4).

See also Figures S4 and S5 and Table S5.

were not degraded in response to UV in the presence of MG132, an inhibitor of the proteasome (Rapić-Otrin et al., 2002) (Figure 5C). The lysine residues at the DDB2 N terminus (aa 5-40), which are targeted by $CRL4^{DDB2}$ for autoubiquitination in vitro, hence regulate the overall cellular concentration of DDB2 in response to UV.

The COP9 Signalosome Mediates Activation between DDB2 and the Ubiquitin Ligase

DDB2 is autoubiquitinated by $CRL4^{DDB2}$ in *cis* irrespective of the presence or absence of DNA damage in vitro. In vivo, however, DDB2 ubiquitination and degradation proceeds in a DNA damage specific fashion. CSN has been implicated in CUL4 inhibition through deneddylation, and is known to dynamically associate with $CRL4^{DDB2}$ complexes (Groisman et al., 2003). Dissociation of the CSN from $CRL4^{DDB2}$ had previously been observed in the presence of nucleosomes (Takedachi et al., 2010). We first examined the effect of CSN on $CRL4^{DDB2}$ autoubiquitination. DDB2, within the $CRL4^{DDB2}$ complex, was readily ubiquitinated in the presence of an E1 (UBA1) and E2 (UbcH5A), as previously observed (Sugasawa et al., 2005). DDB2 autoubiquitination, however, was severely inhibited in the presence of CSN (Figure 5D, lanes 4 and 6). The inhibitory effect of CSN was observed in the presence of wild-type CSN5, or using a CSN5 catalytic mutant deficient in deneddylation (CSN_{ASM}). We then carried out ubiquitination reactions in the presence of irradiated DNA plasmids. Under these conditions CSN, or CSN_{ASM}, no longer protected DDB2 from undergoing autoubiquitination (Figure 5D, lanes 5 and 7). We then examined the DNA specificity of activation. Short duplexes between 15 and 24bp in length containing either THF, 6-4PP or CPD (Figure 5E) were sufficient to overcome CSN inhibition and triggered DDB2 autoubiquitination. Duplexes containing undamaged DNA, on the other hand, did not relieve protection (Figure 5E, lane 6). Analogously, a DDB2 (K244E) mutant defective in damage DNA binding (Wittschieben et al., 2005) was unable to relieve CSN inhibition (Figure 5F). EMSA and equilibrium size-exclusion chromatography indicated that $CRL4^{DDB2}$ dissociated from the CSN-$CRL4^{DDB2}$ in the presence of small damage-containing DNA duplexes (Figure S5). We thereby conclude that substrate binding to the DDB2 subunit of $CRL4^{DDB2}$ triggers CSN release, relieves inhibition and results in an active ligase complex. The DDB2 N terminus subsequently becomes subjected to $CRL4^{DDB2}$ autoubiquitination, which triggers cellular DDB2 degradation in response to UV irradiation.

Previous studies reported a deubiquitination (DUB) enzyme, UBP12, associated with CSN preparation immunopurified from human cells (Zhou et al., 2003). Our recombinant CSN, overexpressed and purified to homogeneity from insect cells (Enchev et al., 2010) (Figure S4) did not show any discernable deubiquitination activity, in the presence or absence of damaged DNA (Figure S4). In addition, while UBP12 DUB activity was previously shown to be inhibited by ubiquitin-aldehyde (Zhou et al., 2003), we observed no such effect on DNA mediated $CRL4^{DDB2}$ activation in the presence of 3.9 μM ubiquitin-aldehyde (Figure 5E, lanes 1 and 2), a concentration that was sufficient to inhibit a control DUB added to the reaction (Figure S5E). The CSN inhibitory properties observed in vitro are therefore intrinsic to the complex and not due to CSN5 mediated deneddylation, or CSN associated DUB activity.

In a minimal, recombinant system we have fully reconstituted DNA damage-dependent activation of $CRL4^{DDB2}$ mediated by CSN (see Figure S5 for mapping of CSN subunits required for protection/release). While the $CRL4^{DDB2}$ complex, as depicted in Figures 3 and 4, is active in the presence of E1 and E2 conjugating enzymes, its activity is inhibited by CSN. The presence of UV damaged DNA serves to relieve CSN inhibition providing a mechanism for DNA dependent activation of the $CRL4^{DDB2}$ ligase.

The CSA DDB1 Complex Reveals a Common Architecture of the DDB1-DCAF Family

DDB2 is a member of the large family of DCAFs, functioning as a DNA damage specific receptor recruiting $CRL4^{DDB2}$ to pyrimidine dimer sites. Additional DCAFs have been described, the majority of which serve as substrate receptors to CRL4 ubiquitin ligases. These receptors likely do not bind DNA, but rather recognize proteins. In the $CRL4^{DDB2}$ structures, DDB2 emerges as modular unit insulated from the CUL4 ligase. The absence of specific interactions between DDB2 and CUL4 would principally allow exchange of DDB2 for other WD40 containing substrate adaptors. We thus focused on the DDB1-CSA-CUL4-RBX1 ($CRL4^{CSA}$) ligase, seemingly unrelated to DDB2 besides the WD40 repeat in its protein sequence, which functions in the transcription-coupled repair (TCR) branch of NER (Fousteri and Mullenders, 2008).

Cockayne syndrome (CS) is a rare congenital disease exhibiting defects in the TCR branch of NER. The stalling of RNAPII observed in the presence of damaged nucleotides tightens the interaction between the RNAPII and the Cockayne syndrome B (CSB) SWI/SNF ATPase. The complex of RNAPII and CSB in turn is a prerequisite for the arrival of the Cockayne syndrome A protein complex ($CRL4^{CSA}$) (Fousteri et al., 2006). Both CSA and CSB are required for successful repair and transcription restart. $CRL4^{CSA}$ has been implicated in the ubiquitination and subsequent degradation of CSB in a UV-dependent fashion (Groisman et al., 2006).

We have determined the structure of the human DDB1-CSA complex at 3.3 Å resolution (Figure 6). The structure was solved by molecular replacement as outlined in Extended Experimental Procedures. CSA comprises a seven-bladed WD40 propeller (aa 30–365) that attaches to DDB1 through a helix-loop-helix motif (aa 1–29). The CSA helix-loop-helix motif (HLH-box) and the WD40 propeller were well ordered, whereas no interpretable electron density was found for the C terminus of CSA (aa 364 to 396) and the C-terminal affinity tag. Irrespective of the limited (20%) sequence identity between DDB2 and CSA, the DDB1-CSA and DDB1-DDB2 complexes show high overall structural similarity (backbone rmsd of 3.4 Å for 355 CSA/DDB2 residues).

The location of CSA patient mutations are indicated in Figure 6B. We note that CSA mutations resulting in milder forms of CS type III (and UV sensitive syndrome $UV^{S}S$) are point mutations expected to cause only limited structural damage. Mutations giving rise to the more severe forms, CS type I and II are point mutations, deletions and premature chain

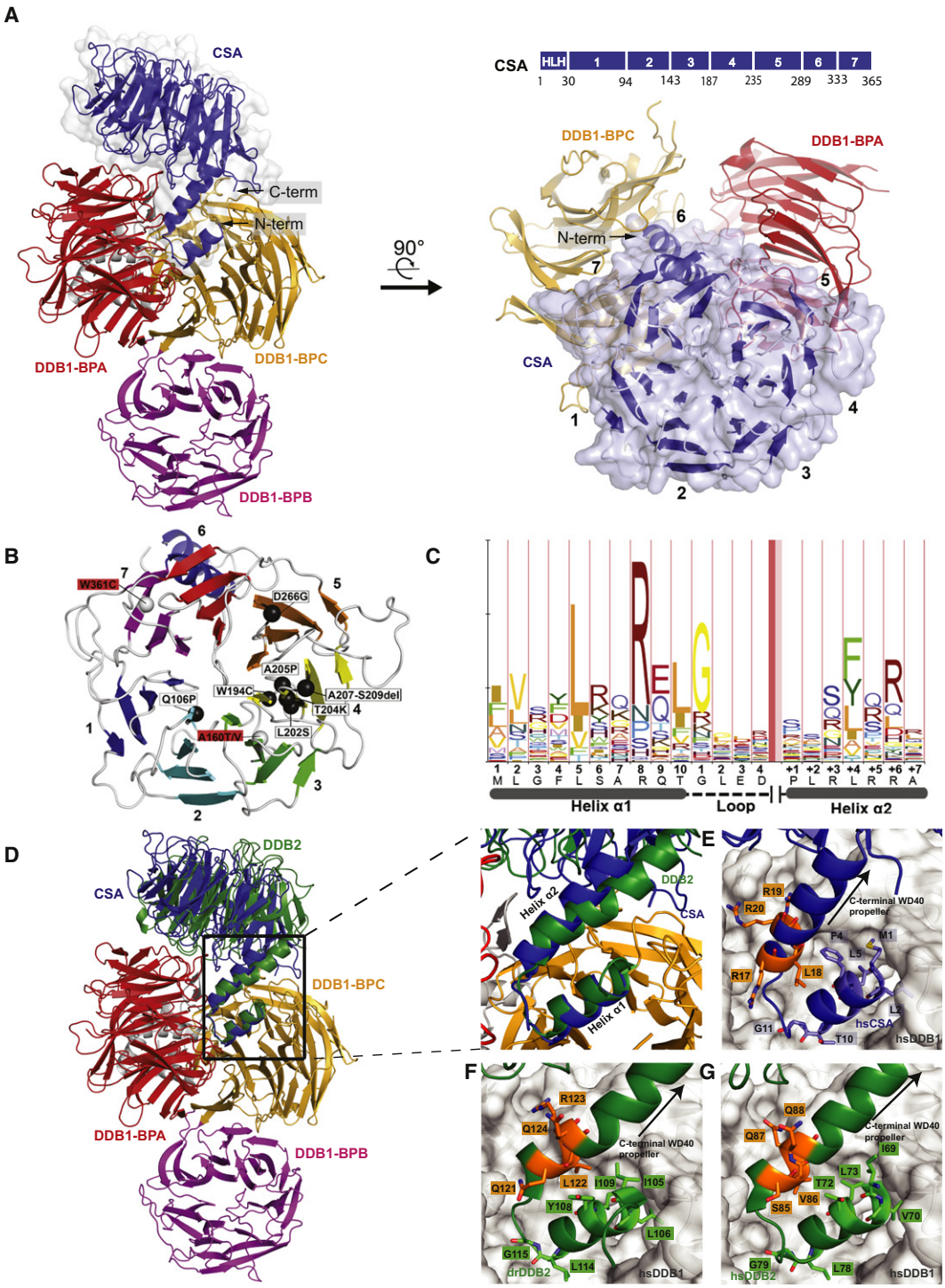

Figure 6. The Structure of DDB1-CSA Suggests a Shared Architecture of CRL4^{DCAF} Complexes

(A) Overall structure of the DDB1-CSA complex. CSA: blue, DDB1 (BPA): red, (BPB): magenta, (BPC): yellow, DDB1-CTD: gray. Schematic overview of the CSA organization.

(B) CSA mutations linked to different phenotypes of Cockayne syndrome (white: CSI, red: CSIII/UV^{S}S).

(C) HMM based sequence logo and corresponding secondary structure of the helix-loop-helix box (see Figure S6A for full alignment).

(D–G) Superposition using DDB1-BPA/BPC results in a similar orientation of CSA (blue) and DDB2 (green) showing the common architecture of the complexes. Close-up view of the helix-loop-helix motif in hsCSA (E), drDDB2 (F) and hsDDB2 (G), respectively. Residues belonging to the conserved motif are indicated. See also Figures S6 and S7 and Table S6.

termination mutations expected to severely compromise the CSA structure (see Table S6 for detailed analysis of CSA patient mutations and discussion of structure and phenotype correlations).

The CSA-DDB1 Interaction Is Mediated through the HLH-BOX

DDB1 comprises three WD40 domains (BPA, BPB and BPC) and a C-terminal α-helical domain (CTD). We found that CSA binds to DDB1 with an N-terminal HLH-box segment formed by aa 1–29 (Figures 6A and 6D). The HLH-box localizes to a cleft between the DDB1 propellers BPA and BPC. The two parallel HLH-box helices, α1 and α2, pack against each other. The HLH-box interaction surface with DDB1 encompasses the outer surface of α1 and the N-terminal tip of α2 (aa 16–20). The majority of CSA α1 interactions with DDB1 are hydrophobic (CSA Met1, Leu5), or contact DDB1 through H-bonds (CSA Ser6, Arg8, Gln9). While α1 is buried deeply in the BPC DDB1 propeller, α2 is further detached from DDB1 pointing toward the DDB1 (BPA) propeller. CSA α2, contacts DDB1 largely through H-bonds and long-range salt bridges comprising CSA α2 residues Arg17 and Arg20, respectively.

Analysis of Helix-Loop-Helix Motifs Identified in Other WD40-Containing DCAFs

The unexpected structural similarity between DDB2 and CSA prompted us to reinvestigate whether the majority of WD40 containing DCAFs bind DDB1 in a similar fashion. In proteomic studies approximately 50 WD40-containing DCAFs proteins were identified as putative substrate receptors (Angers et al., 2006; Bennett et al., 2010; He et al., 2006; Higa et al., 2006; Jin et al., 2006). Out of the 18 WD40-containing DCAFs, identified in at least two proteomic studies, 13 contained an HLH-box (Figure S6A). In addition to the conserved α1 helix (Fukumoto et al., 2008; Li et al., 2010) (Figures 6D–6G), we now also detect conservation for helix α2. The beginning of α2 (residues +1 to +3) is composed of small and hydrophilic side chains, followed by large hydrophobic residues (Phe, Leu and Tyr) at the +4 position, which pack against α1 (Figure 6C). A large, often polar, residue is found in the +6 position interacting with DDB1 (BPA). The length of the loop between α1 and α2 appears nonconserved and varies between 2 and 7 residues.

Based on these sequence signatures, we identify DDB1-(WD40) DCAF family members CDT2, DCAF1, WDR21, WDR23, WDR40, WDR22, WDR32, and PHIP among others (Figure S6) as having a HLH-box predicted to bind DDB1 in a manner similar to DDB2 and CSA. The resultant $CRL4^{DCAF(WD40)}$ complexes are expected to strongly resemble $CRL4^{DDB2}$ sharing principle properties such as ligase mobility (see Figure S6C for a model of $CRL4^{CSA}$).

We then tested the functional interplay between $CRL4^{CSA}$ and CSN in vitro. We observed that CSA is also autoubiquitinated in vitro (Figure 7A, lane 2) and that CSA autoubiquitination is in turn inhibited by the addition of CSN (or CSN_{ASM}) (Figure 7A, lane 3 and 5). Providing the $CRL4^{CSA}$ substrate CSB relieved CSN inhibition, and led to ubiquitination of CSB and CSA (Figure 7A, lanes 4, 6, and 7, and Figure 7B). In a fully recombinant in vitro system, damage DNA binding to $CRL4^{DDB2}$, as well as CSB binding to $CRL4^{CSA}$, displaces CSN resulting in activation of the CRL4 ligase complex.

The overall functional and regulatory constraints following from the $CRL4^{DDB2}$ (and $CRL4^{CSA}$) architectures thus likely extend to other members of the $CRL4^{DCAF}$ family.

DISCUSSION

The Molecular Basis of Targeting, Recruitment, and Activation of the $CRL4^{DDB2}$ Ligase in Chromatin

On the basis of our findings, we propose the following working model for $CRL4^{DDB2}$ recruitment and activation in response to UV damage (Figure 7C): In the absence of DNA damage, nuclear $CRL4^{DDB2}$ is complexed to CSN in a nonchromatin-bound form (Groisman et al., 2003). Following UV damage, $CRL4^{DDB2}$-CSN is recruited to DNA by its ability to interrogate nucleosomes for the presence of 6-4PP and CPD lesions (Figure 2). $CRL4^{DDB2}$ is structurally optimized for recognition of CPDs, which due to their small intrinsic helix destabilization frequently escape detection by other damage surveillance factors (Figure 1). XPC-RAD23, alone, has no significant affinity for CPD and is unable to detect 6-4PP lesions in chromatin (Yasuda et al., 2005). Yet XPC is essential for efficient NER repair. The ability of $CRL4^{DDB2}$ to recognize 6-4PPs, and particularly CPDs, embedded in nucleosomes provides a pathway to recruit XPC to lesions in chromatin and activate the ligase thus facilitating NER (Sugasawa, 2006). We find that DNA damage binding to DDB2 directly displaces CSN from $CRL4^{DDB2}$ resulting in ligase activation (Figure 5). Active $CRL4^{DDB2}$ targets histones, XPC and possibly additional proteins located within ~100 Å around the lesion for ubiquitination. The release of CSN additionally allows $CRL4^{DDB2}$ to autoubiquitinate its DDB2 subunit on the N terminus (Figure 4). This results in degradation of DDB2 and may function as a timing device delimiting $CRL4^{DDB2}$ activity following UV. A $CRL4^{DDB2}$ variant defective in DNA binding, as seen in patient XP82TO, retains CSN binding and does not undergo autoubiquitination and degradation following UV in vivo (Rapić-Otrin et al., 2002; Wittschieben et al., 2005; Takedachi et al., 2010) (Figure 5F).

The Architecture of the $CRL4^{DCAF}$ Family

The $CRL4^{DDB2}$ ligase is perceived to be a special case, as it recognizes a nonprotein substrate. The ligand, in this case DNA, is atypically not the target for ubiquitination, but rather proteins in its proximity are the entities ubiquitinated. In order to examine how other $CRL4^{DCAF}$ complexes, structurally and functionally, relate to $CRL4^{DDB2}$, we determined the structure of the DDB1-CSA complex. The DDB1-CSA complex, which was shown to bind a protein epitope rather than damaged DNA (Groisman et al., 2006) revealed a surprising overall architectural similarity to the DDB1-DDB2 complex. We find that CSN mediated inhibition of $CRL4^{CSA}$ is released through addition of CSB, similar to what has been observed for $CRL4^{DDB2}$. In vivo, the disappearance of CSN from the $CRL4^{CSA}$ complex (ca. 4 hr post-UV) coincides with ubiquitination and disappearance of CSB (Groisman et al., 2006). Structure-based sequence analysis identified a common HLH motif within the WD40-DCAF family expected to link other WD40 containing DCAFs to DDB1 in a

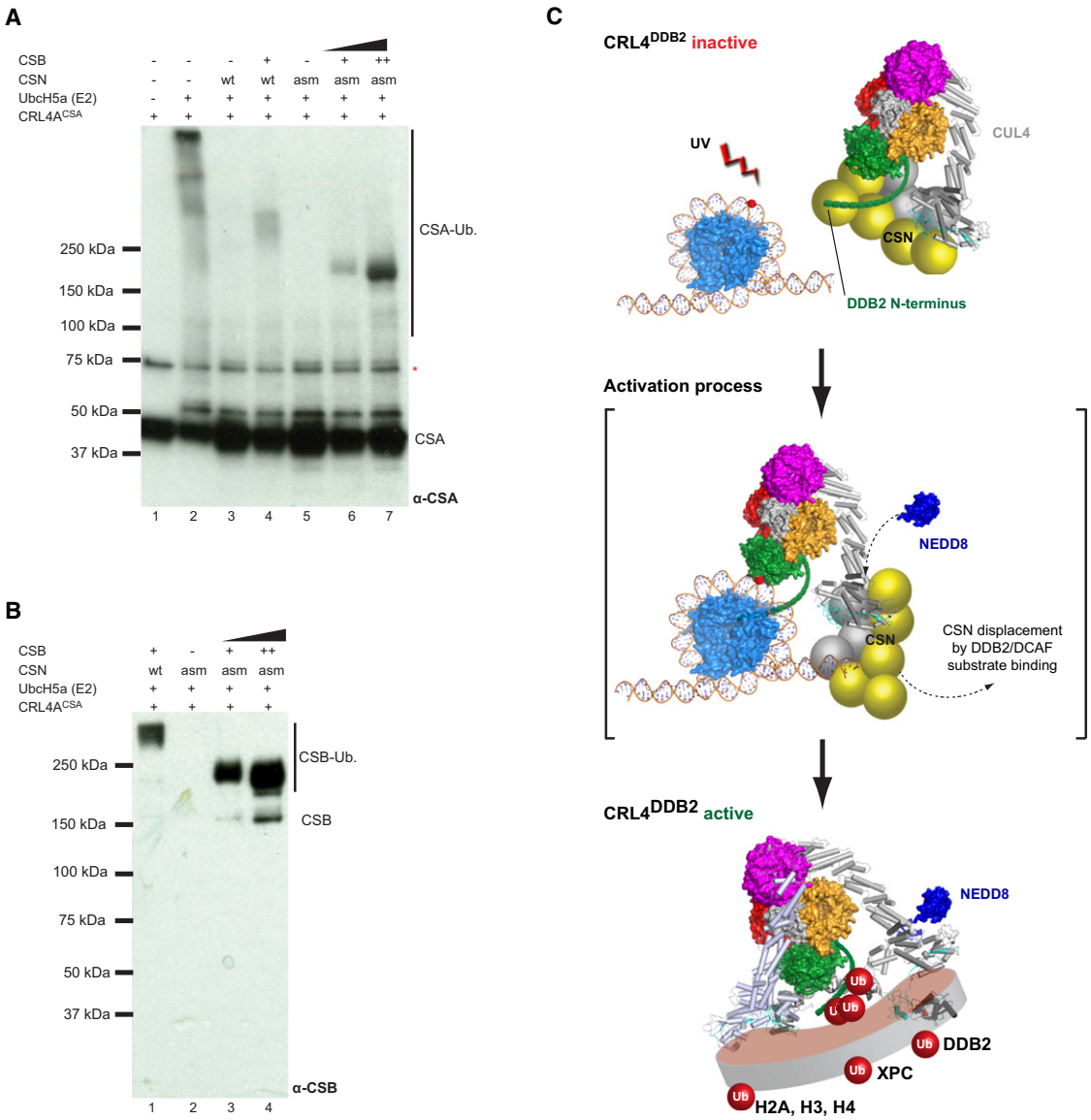

Figure 7. Model for CRL4^{DDB2} Ligase Activation and Release of CSN upon Damage Binding

(A) In vitro ubiquitination assays were performed with CRL4A^{CSA} complex and analyzed by CSA immunoblot. Wild-type COP9 signalosome (CSN) complex (lane 3) or a complex containing a CSN5 active site mutant (lane 5) significantly inhibited CSA autoubiquitination. This inhibition was relieved by the addition of CSB to the reaction (lanes 4, 6, and 7). Unspecific crossreactivity of the anti-CSA antibody is indicated with a red asterisk. CSB immunoblotting demonstrated that the CSB substrate is also ubiquitinated in this reaction (B). (C) In complex with CSN, CRL4^{DDB2} is held in a ubiquitin ligase inactive state. UV irradiation induces lesion formation in chromatin and recruitment of the CRL4^{DDB2}-CSN complex to the site of damage. It is currently not clear if DDB2 binds on the nucleosome, or to a looped off intermediate (Duan and Smerdon, 2010). Binding to chromatin/nucleosome results in steric displacement of CSN (involving CSN subunits 1,2,3,4, and 6) and ligase activation. This in turn allows for ubiquitination of diverse substrates within the zone of ubiquitination including histones, XPC and DDB2.

manner similar to that of CSA and DDB2. At present, we can not exclude that alternative DCAF binding modes exist, or that access of the DCAF HLH-box to DDB1 is subject to regulation. Our results demonstrate that CRL4^{DDB2}, CRL4^{CSA} and with it the majority of CRL4$^{DCAF/WD40}$ complexes are predicted, to share a common architectural scaffold. These CRL4 ligases are expected to exhibit mobility, and hence, absence of direct crosstalk between the DCAF substrate receptor and the ubiquitin ligase, requiring CSN to mediate activation.

Substrate-Dependent Crosstalk between CRL4 Complexes and the COP9 Signalosome

CSN is a key regulator of cullin-RING ligase activity. The involvement of CSN in ligase regulation poses the following question: how is a specific ligase regulated by CSN, without affecting the remainder of cullin-RING ligases. We find that the association and inhibition of CRL4^{DDB2} by CSN is relieved upon DNA damage binding to the WD40 propeller of DDB2 (Figure 5). A similar behavior is seen for CRL4^{CSA} where CSB binding

displaces CSN (Figures 7A and 7B). Indeed, we observe in CRL4^{DDB2}-CSN negative stained EM single particle reconstructions that the DDB2 subunit is held in close proximity to CSN (data not shown). Other structurally related CRL4^{DCAF} complexes are thus expected to bind CSN in a similar fashion. This strongly suggests that CSN release and subsequent activation of CRL4^{DCAF} complexes are simply triggered by substrate binding to the DCAF within the CRL4^{DCAF}-CSN complex.

Protection of substrate receptors by CSN has previously been described for the CRL1 and CRL3 families in vivo (Bornstein et al., 2006; Schmidt et al., 2009; Zhou et al., 2003) and likely extends to the CRL4 family (Bennett et al., 2010). The protective effect of CSN on DDB2 autoubiquitination observed in this study is independent of deubiquitinating enzymes, and does not require CSN5 mediated deneddylation (see Figure S5 for CSN subunits required for inhibition). Similar properties have been observed for the CSN-CRL4^{CSA} interplay, although the cellular role of CSA autoubiquitination is unclear at present. In vivo, (1) the intrinsic CSN deneddylase activity, (2) CSN-associated deubiquitinases, and (3) the nonenzymatic CSN inhibition observed are all expected to act in concert inhibiting CRL4 in the absence of an activating cue. Further work is needed to define the relative contribution of these three strategies (1–3) to CSN mediated inhibition in vivo. However, all three levels of inhibition are simultaneously relieved once DDB2 (CSA) contacts DNA damage (CSB), as the direct contact between receptor and substrate results in CSN dissociation and loss of receptor protection. In light of the conserved architecture of the majority of CRL4$^{DCAF(WD40)}$ complexes this provides a general mechanism for regulating the CRL4 CSN interplay.

EXPERIMENTAL PROCEDURES

Protein Expression and Purification

All proteins used for structure determination were cloned into pFastBac Dual vectors (Invitrogen) and expressed and purified from High Five cells (Invitrogen) as outlined in Scrima et al., 2008 (see also Extended Experimental Procedures). Purified recombinant CSB protein was provided as a kind gift from Regina Groisman. Enzymes for neddylation such as NAE1/UBA3 and UbcH12, as well as NEDD8, were purified as N-terminal His_6 fusion proteins from *Escherichia coli* (Duda et al., 2008). hsUBA1, hsUbcH5A, hsUbcH5B, hsUbiquitin and hsUbiquitin-K0 were purchased from Boston Biochem.

Oligonucleotides Used in This Study

Single stranded DNA oligonucleotides and oligonucleotides containing tetrahydrofuran (THF) lesion were purchased from Sigma Aldrich. Oligonucleotides containing the cis-syn CPD were synthesized using phosphor-amidite building blocks (Glenn Research, USA). Sequences of oligonucleotides used are provided in the Tables S4 and S5.

Crystallization and Structure Solution

Crystallization conditions as well as data collection and refinement statistics are given in Table S1.

Cellular Assays

HA-tagged DDB2 (wild-type or mutant) was stably overexpressed in a normal human fibroblast cell line, WI38 VA13, by using the pIREShyg vector. The transformed cells were exposed to UVC (10 J/m^2) and incubated for various times. Whole-cell extracts were prepared and analyzed by immunoblotting.

In Vitro Ubiquitination Assays

Assays for autoubiquitination were carried out as described in Sugasawa, 2006. Antibodies used include α-hsDDB2 (AF3297, R&D Biosystems), α-XPC (Sugasawa et al., 2005), α-CSA (GTX100145, GeneTex), α-CSB (SC10458, Santa Cruz) and horseradish peroxidase (HRP)-conjugated secondary antibodies against Goat IgG (R&D Biosystems) and rabbit IgG (GeneTex).

ACCESSION NUMBERS

The following structural coordinates have been reported: CPD#1(pdb:4A08), CPD#2(pdb:4A09), CPD#3(pdb:4A0A), CPD#4(pdb: 4A0B), CAND1-CUL4B (pdb:4A0C), CRL4A^{DDB2}-DNA(pdb:4A0K), CRL4B^{DDB2}-DNA(pdb:4A0L), and DDB1-CSA(pdb:4A11).

SUPPLEMENTAL INFORMATION

Supplemental Information includes Extended Experimental Procedures, six tables, and seven figures and can be found with this article online at doi:10.1016/j.cell.2011.10.035.

ACKNOWLEDGMENTS

This work was supported by the Novartis Research Foundation and grants to N.H.T. from the European Research Council (ERC-2010-StG 260481-MoBaCS), OncoSuisse (OCS-02365-02-2009), and the Swiss National Science Foundation (31003A_120205); an SNF Ambizione Grant (A.S.), an EMBO STF (E.S.F.), and Novartis Presidential Fellowship (G.M.L.). K.S. was supported by Grants-in-Aid from the Ministry of Education, Culture, Sports, Science, and Technology of Japan and by the Takeda Science Foundation. We thank Susan Gasser, Dirk Schübeler, Lukas Leder, Martin Renatus, and Philip Jeffrey for help and discussion. We are grateful to Daniel Hess and Dominique Klein (FMI protein analysis facility) for carrying out the mass-spectrometric analysis. Part of this work was performed at the Swiss Light Source at the Paul Scherrer Institut, Villigen, Switzerland.

Received: June 28, 2011
Revised: August 12, 2011
Accepted: October 16, 2011
Published: November 23, 2011

REFERENCES

Aboussekhra, A., Biggerstaff, M., Shivji, M.K., Vilpo, J.A., Moncollin, V., Podust, V.N., Protić, M., Hübscher, U., Egly, J.M., and Wood, R.D. (1995). Mammalian DNA nucleotide excision repair reconstituted with purified protein components. Cell *80*, 859–868.

Angers, S., Li, T., Yi, X., MacCoss, M.J., Moon, R.T., and Zheng, N. (2006). Molecular architecture and assembly of the DDB1-CUL4A ubiquitin ligase machinery. Nature *443*, 590–593.

Batty, D., Rapic Otrin, V., Levine, A., and Wood, R. (2000). Stable binding of human XPC complex to irradiated DNA confers strong discrimination for damaged sites. J. Mol. Biol. *300*, 275–290.

Bennett, E.J., Rush, J., Gygi, S.P., and Harper, J.W. (2010). Dynamics of cullin-RING ubiquitin ligase network revealed by systematic quantitative proteomics. Cell *143*, 951–965.

Bornstein, G., Ganoth, D., and Hershko, A. (2006). Regulation of neddylation and deneddylation of cullin1 in SCFSkp2 ubiquitin ligase by F-box protein and substrate. Proc. Natl. Acad. Sci. USA *103*, 11515–11520.

Brunger, A., Adams, P., Clore, G., DeLano, W., Gros, P., Grosse-Kunstleve, R., Jiang, J., Kuszewski, J., Nilges, M., Pannu, N., et al. (1998). Crystallography & NMR system: A new software suite for macromolecular structure determination. Acta Crystallogr. D Biol. Crystallogr. *54*, 905–921.

Creighton, T.E. (1992). Proteins: Structures and Molecular Properties, second edition (W. H. Freeman and Company).

Duan, M.-R., and Smerdon, M.J. (2010). UV damage in DNA promotes nucleosome unwrapping. J. Biol. Chem. *285*, 26295–26303.

Duda, D., Borg, L., Scott, D., Hunt, H., Hammel, M., and Schulman, B. (2008). Structural insights into NEDD8 activation of cullin-RING ligases: conformational control of conjugation. Cell *134*, 995–1006.

Enchev, R.I., Schreiber, A., Beuron, F., and Morris, E.P. (2010). Structural insights into the COP9 signalosome and its common architecture with the 26S proteasome lid and eIF3. Structure *18*, 518–527.

Fousteri, M., and Mullenders, L.H.F. (2008). Transcription-coupled nucleotide excision repair in mammalian cells: molecular mechanisms and biological effects. Cell Res. *18*, 73–84.

Fousteri, M., Vermeulen, W., van Zeeland, A.A., and Mullenders, L.H. (2006). Cockayne syndrome A and B proteins differentially regulate recruitment of chromatin remodeling and repair factors to stalled RNA polymerase II in vivo. Mol. Cell *23*, 471–482.

Friedberg, E.C. (2001). How nucleotide excision repair protects against cancer. Nat. Rev. Cancer *1*, 22–33.

Fukumoto, Y., Dohmae, N., and Hanaoka, F. (2008). Schizosaccharomyces pombe Ddb1 recruits substrate-specific adaptor proteins through a novel protein motif, the DDB-box. Mol. Cell. Biol. *28*, 6746–6756.

Furukawa, M., Zhang, Y., McCarville, J., Ohta, T., and Xiong, Y. (2000). The CUL1 C-terminal sequence and ROC1 are required for efficient nuclear accumulation, NEDD8 modification, and ubiquitin ligase activity of CUL1. Mol. Cell. Biol. *20*, 8185–8197.

Gale, J.M., and Smerdon, M.J. (1988). Photofootprint of nucleosome core DNA in intact chromatin having different structural states. J. Mol. Biol. *204*, 949–958.

Groisman, R., Kuraoka, I., Chevallier, O., Gaye, N., Magnaldo, T., Tanaka, K., Kisselev, A.F., Harel-Bellan, A., and Nakatani, Y. (2006). CSA-dependent degradation of CSB by the ubiquitin-proteasome pathway establishes a link between complementation factors of the Cockayne syndrome. Genes Dev. *20*, 1429–1434.

Groisman, R., Polanowska, J., Kuraoka, I., Sawada, J., Saijo, M., Drapkin, R., Kisselev, A., Tanaka, K., and Nakatani, Y. (2003). The ubiquitin ligase activity in the DDB2 and CSA complexes is differentially regulated by the COP9 signalosome in response to DNA damage. Cell *113*, 357–367.

Guerrero-Santoro, J., Kapetanaki, M., Hsieh, C., Gorbachinsky, I., Levine, A., and Rapic-Otrin, V. (2008). The cullin 4B-based UV-damaged DNA-binding protein ligase binds to UV-damaged chromatin and ubiquitinates histone H2A. Cancer Res. *68*, 5014–5022.

Hannss, R., and Dubiel, W. (2011). COP9 signalosome function in the DDR. FEBS Lett. *585*, 2845–2852.

He, Y., McCall, C., Hu, J., Zeng, Y., and Xiong, Y. (2006). DDB1 functions as a linker to recruit receptor WD40 proteins to CUL4-ROC1 ubiquitin ligases. Genes Dev. *20*, 2949–2954.

Higa, L., Wu, M., Ye, T., Kobayashi, R., Sun, H., and Zhang, H. (2006). CUL4-DDB1 ubiquitin ligase interacts with multiple WD40-repeat proteins and regulates histone methylation. Nat. Cell Biol. *8*, 1277–1283.

Hoeijmakers, J.H.J. (2009). DNA damage, aging, and cancer. N. Engl. J. Med. *361*, 1475–1485.

Hwang, B.J., Toering, S., Francke, U., and Chu, G. (1998). p48 Activates a UV-damaged-DNA binding factor and is defective in xeroderma pigmentosum group E cells that lack binding activity. Mol. Cell. Biol. *18*, 4391–4399.

Jackson, S., and Xiong, Y. (2009). CRL4s: the CUL4-RING E3 ubiquitin ligases. Trends Biochem. Sci. *34*, 562–570.

Jin, J., Arias, E., Chen, J., Harper, J., and Walter, J. (2006). A family of diverse Cul4-Ddb1-interacting proteins includes Cdt2, which is required for S phase destruction of the replication factor Cdt1. Mol. Cell *23*, 709–721.

Jing, Y., Kao, J.F., and Taylor, J.S. (1998). Thermodynamic and base-pairing studies of matched and mismatched DNA dodecamer duplexes containing cis-syn, (6-4) and Dewar photoproducts of TT. Nucleic Acids Res. *26*, 3845–3853.

Kapetanaki, M.G., Guerrero-Santoro, J., Bisi, D.C., Hsieh, C.L., Rapić-Otrin, V., and Levine, A.S. (2006). The DDB1-CUL4ADDB2 ubiquitin ligase is deficient in xeroderma pigmentosum group E and targets histone H2A at UV-damaged DNA sites. Proc. Natl. Acad. Sci. USA *103*, 2588–2593.

Krissinel, E., and Henrick, K. (2007). Inference of macromolecular assemblies from crystalline state. J. Mol. Biol. *372*, 774–797.

Lee, J., and Zhou, P. (2007). DCAFs, the missing link of the CUL4-DDB1 ubiquitin ligase. Mol. Cell *26*, 775–780.

Li, T., Chen, X., Garbutt, K.C., Zhou, P., and Zheng, N. (2006). Structure of DDB1 in complex with a paramyxovirus V protein: viral hijack of a propeller cluster in ubiquitin ligase. Cell *124*, 105–117.

Li, T., Robert, E.I., van Breugel, P.C., Strubin, M., and Zheng, N. (2010). A promiscuous α-helical motif anchors viral hijackers and substrate receptors to the CUL4-DDB1 ubiquitin ligase machinery. Nat. Struct. Mol. Biol. *17*, 105–111.

Luijsterburg, M.S., Goedhart, J., Moser, J., Kool, H., Geverts, B., Houtsmuller, A.B., Mullenders, L.H.F., Vermeulen, W., and van Driel, R. (2007). Dynamic in vivo interaction of DDB2 E3 ubiquitin ligase with UV-damaged DNA is independent of damage-recognition protein XPC. J. Cell Sci. *120*, 2706–2716.

Mitchell, D.L., Adair, G.M., and Nairn, R.S. (1989). Inhibition of transient gene expression in Chinese hamster ovary cells by triplet-sensitized UV-B irradiation of transfected DNA. Photochem. Photobiol. *50*, 639–646.

Moser, J., Volker, M., Kool, H., Alekseev, S., Vrieling, H., Yasui, A., van Zeeland, A., and Mullenders, L. (2005). The UV-damaged DNA binding protein mediates efficient targeting of the nucleotide excision repair complex to UV-induced photo lesions. DNA Repair (Amst.) *4*, 571–582.

Nishi, R., Alekseev, S., Dinant, C., Hoogstraten, D., Houtsmuller, A.B., Hoeijmakers, J.H., Vermeulen, W., Hanaoka, F., and Sugasawa, K. (2009). UV-DDB-dependent regulation of nucleotide excision repair kinetics in living cells. DNA Repair (Amst.) *8*, 767–776.

Payne, A., and Chu, G. (1994). Xeroderma pigmentosum group E binding factor recognizes a broad spectrum of DNA damage. Mutat. Res. *310*, 89–102.

Rapić-Otrin, V., McLenigan, M.P., Bisi, D.C., Gonzalez, M., and Levine, A.S. (2002). Sequential binding of UV DNA damage binding factor and degradation of the p48 subunit as early events after UV irradiation. Nucleic Acids Res. *30*, 2588–2598.

Schmidt, M.W., McQuary, P.R., Wee, S., Hofmann, K., and Wolf, D.A. (2009). F-box-directed CRL complex assembly and regulation by the CSN and CAND1. Mol. Cell *35*, 586–597.

Scrima, A., Fischer, E.S., Lingaraju, G.M., Böhm, K., Cavadini, S., and Thomä, N.H. (2011). Detecting UV-lesions in the genome: The modular CRL4 ubiquitin ligase does it best! FEBS Lett. *585*, 2818–2825.

Scrima, A., Konícková, R., Czyzewski, B.K., Kawasaki, Y., Jeffrey, P.D., Groisman, R., Nakatani, Y., Iwai, S., Pavletich, N.P., and Thomä, N.H. (2008). Structural basis of UV DNA-damage recognition by the DDB1-DDB2 complex. Cell *135*, 1213–1223.

Sugasawa, K. (2006). UV-induced ubiquitylation of XPC complex, the UV-DDB-ubiquitin ligase complex, and DNA repair. J. Mol. Histol. *37*, 189–202.

Sugasawa, K. (2010). Regulation of damage recognition in mammalian global genomic nucleotide excision repair. Mutat. Res. *685*, 29–37.

Sugasawa, K., Okamoto, T., Shimizu, Y., Masutani, C., Iwai, S., and Hanaoka, F. (2001). A multistep damage recognition mechanism for global genomic nucleotide excision repair. Genes Dev. *15*, 507–521.

Sugasawa, K., Okuda, Y., Saijo, M., Nishi, R., Matsuda, N., Chu, G., Mori, T., Iwai, S., Tanaka, K., Tanaka, K., et al. (2005). UV-Induced Ubiquitylation of XPC Protein Mediated by UV-DDB-Ubiquitin Ligase Complex. Cell *121*, 387–400.

Takedachi, A., Saijo, M., and Tanaka, K. (2010). DDB2 complex-mediated ubiquitylation around DNA damage is oppositely regulated by XPC and Ku and contributes to the recruitment of XPA. Mol. Cell. Biol. *30*, 2708–2723.

Tang, J., and Chu, G. (2002). Xeroderma pigmentosum complementation group E and UV-damaged DNA-binding protein. DNA Repair (Amst.) *1*, 601–616.

Tang, J.Y., Hwang, B.J., Ford, J.M., Hanawalt, P.C., and Chu, G. (2000). Xeroderma pigmentosum p48 gene enhances global genomic repair and suppresses UV-induced mutagenesis. Mol. Cell *5*, 737–744.

Tornaletti, S. (2009). DNA repair in mammalian cells: Transcription-coupled DNA repair: directing your effort where it's most needed. Cell. Mol. Life Sci. *66*, 1010–1020.

Troelstra, C., van Gool, A., de Wit, J., Vermeulen, W., Bootsma, D., and Hoeijmakers, J.H. (1992). ERCC6, a member of a subfamily of putative helicases, is involved in Cockayne's syndrome and preferential repair of active genes. Cell *71*, 939–953.

Volker, M., Mone, M., Karmakar, P., van Hoffen, A., Schul, W., Vermeulen, W., Hoeijmakers, J., van Driel, R., van Zeeland, A., and Mullenders, L. (2001). Sequential assembly of the nucleotide excision repair factors in vivo. Mol. Cell *8*, 213–224.

Wang, H., Zhai, L., Xu, J., Joo, H., Jackson, S., Erdjument-Bromage, H., Tempst, P., Xiong, Y., and Zhang, Y. (2006). Histone H3 and H4 ubiquitylation by the CUL4-DDB-ROC1 ubiquitin ligase facilitates cellular response to DNA damage. Mol. Cell *22*, 383–394.

Wittschieben, B., Iwai, S., and Wood, R. (2005). DDB1-DDB2 (xeroderma pigmentosum group E) protein complex recognizes a cyclobutane pyrimidine dimer, mismatches, apurinic/apyrimidinic sites, and compound lesions in DNA. J. Biol. Chem. *280*, 39982–39989.

Yasuda, T., Sugasawa, K., Shimizu, Y., Iwai, S., Shiomi, T., and Hanaoka, F. (2005). Nucleosomal structure of undamaged DNA regions suppresses the nonspecific DNA binding of the XPC complex. DNA Repair (Amst.) *4*, 389–395.

Zhou, C., Wee, S., Rhee, E., Naumann, M., Dubiel, W., and Wolf, D.A. (2003). Fission yeast COP9/signalosome suppresses cullin activity through recruitment of the deubiquitylating enzyme Ubp12p. Mol. Cell *11*, 927–938.